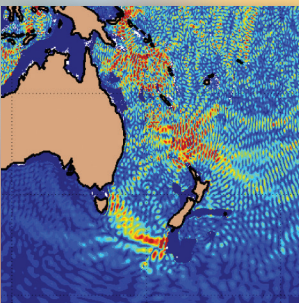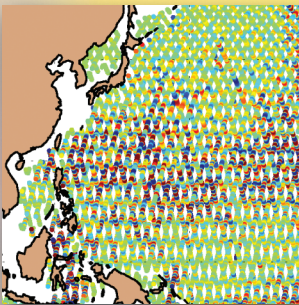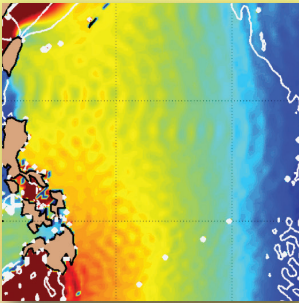# Global Modeling of Internal Tides

Within an Eddying Ocean General Circulation Model

BY BRIAN K. ARBIC, JAMES G. RICHMAN, JAY F. SHRIVER,
PATRICK G. TIMKO, E. JOSEPH METZGER, AND ALAN J. WALLCRAFT

ABSTRACT. Ocean tides, and the atmospherically forced oceanic general circulation and its associated mesoscale eddy field, have long been run separately in high-resolution global models. They are now being simulated concurrently in a high-resolution version of the HYbrid Coordinate Ocean Model (HYCOM). The incorporation of horizontally varying stratification with the addition of atmospheric forcing yields internal tides (internal waves of tidal frequency) in high-latitude, low-stratification regions that are qualitatively different from those in earlier global internal tide models, in which atmospheric forcing and horizontally variable stratification were absent. The internal tides in the new concurrent HYCOM simulations compare well with those measured in along-track satellite altimeter data. The new concurrent simulations demonstrate that the wavenumber spectrum of sea surface height—a measure of the energy contained in different length scales—is dominated in some locations by internal tides and in others by mesoscale eddies. Tidal kinetic energies in the new concurrent simulations compare well with those in current-meter observations, as long as sufficient spatial averaging is performed. The new concurrent simulations are being used in the planning of future-generation satellite altimeters, in the provision of boundary conditions for coastal ocean models, and in studies of ocean mixing.

TIDES AND GLOBAL TIDE MODELING

Ocean tides result from the difference in the gravitational potential of the Moon and Sun across Earth's extent (Cartwright, 1999). The tidal potential, or equilibrium tide, has a simple shape first elucidated by Newton. Actual ocean tides represent a complex dynamical response, first elucidated in mathematical form by Laplace, to the equilibrium tidal forcing. Ocean tides are affected by several factors, including Earth's rotation, friction with the seafloor, water depth (which controls the speed of shallow-water gravity waves), and the presence of continents, as well as seemingly exotic effects such as tides in the solid Earth and perturbations in the gravitational self-attraction of mass in the ocean and solid Earth brought about by tidal motions (Hendershott, 1972).

The shallow-water equations used by modern scientists to model ocean tides are essentially updated versions of the Laplace tidal equations, in which the effects described above are included. An important assumption in the shallow-water equations is that motions have horizontal scales that are large compared to the water depth and therefore lie in hydrostatic balance (Pedlosky, 1987; Vallis, 2006).

Early global models of the tides (e.g., Hendershott, 1972) were barotropic, meaning that the relatively small variations in ocean density from the top to the bottom of the water column were ignored. In a shallow-water model, the assumption of constant density implies that the horizontal velocities do not change with vertical position in the water column, though they do change with latitude and longitude. The spacing between adjacent horizontal grid points in early global tide models was about 6° (670 km). This relatively coarse grid spacing was dictated by the limited computer power available at the time. Modern computer power allows computation of the global tides for grid spacing as fine as 1/25°–1/12° (4.4–8.9 km).

As has been recognized for some time (e.g., Wunsch, 1975), tidal flow over topographic features generates an internal tide. In a stratified fluid, the vertical motions induced by flow over topography take the form of internal waves (waves along interfaces between fluids of differing densities), which are the subject of this special issue of *Oceanography*. Internal tides are internal waves with tidal frequencies. Internal tides can have displacement amplitudes greater than 50 m and current speeds greater than 2 m s^{-1}. Internal tides are a topic of great current interest, for a number of reasons. The vertical motions (displacements) associated with internal tides affect the motions of gliders, floats, and other oceanographic instruments. They also impact the motions of submarines and acoustic (sound) waves in the ocean. Most importantly, the breaking of internal waves is a leading source of mixing, and internal tides are thought to be one of the largest energy sources powering mixing in the deep ocean. It is therefore thought that tides exert important controls on the stratification and circulation of the deep ocean (Munk and Wunsch, 1998).

Internal tides have much smaller horizontal scales than barotropic tides, and by definition can only be numerically modeled in a system with more than one layer in the vertical direction. Because both horizontal and vertical resolution must be increased, the computational effort required to model internal tides is commensurately greater than the effort required to model barotropic tides. One approach to this challenge is to model internal tides on a regional scale, which permits higher spatial resolution than is possible in global models. Carter et al. (2012, in this issue) provide a review of regional internal tide models. Because of the great computational expense involved in global internal tide models, the first papers on global modeling of internal tides are less than a decade old, and the number of published papers that focus on, or at least include, global models of internal tides is, to the best of our knowledge, still quite small (Arbic et al., 2004; Simmons et al., 2004; Hibiya et al., 2006; Simmons, 2008; Arbic et al., 2010; Niwa and Hibiya, 2011). In the earliest global internal tide modeling

Brian K. Arbic *(arbic@umich.edu) is Assistant Professor, Department of Earth and Environmental Sciences, University of Michigan, Ann Arbor, MI, USA.* **James G. Richman** *is Oceanographer, Ocean Dynamics and Prediction Branch, Naval Research Laboratory, Stennis Space Center, MS, USA.* **Jay F. Shriver** *is Oceanographer, Ocean Dynamics and Prediction Branch, Naval Research Laboratory, Stennis Space Center, MS, USA.* **Patrick G. Timko** *is Postdoctoral Fellow, Department of Earth and Environmental Sciences, University of Michigan, Ann Arbor, MI, USA.* **E. Joseph Metzger** *is Meteorologist, Ocean Dynamics and Prediction Branch, Naval Research Laboratory, Stennis Space Center, MS, USA.* **Alan J. Wallcraft** *is Computer Scientist, Ocean Dynamics and Prediction Branch, Naval Research Laboratory, Stennis Space Center, MS, USA.*

studies, astronomical tidal forcing was the only forcing present in the model. Due to the lack of atmospheric forcing, which sets the oceanic stratification, the oceanic stratification was assumed to be horizontally uniform. Oceanic stratification in subtropical regions was assumed to hold everywhere in the ocean and, as a result, the internal tides in polar regions in early global internal tide models were noted to be quite inaccurate (Padman et al., 2006).

As in many subdisciplines of physical oceanography, the study of tides has been revolutionized by the advent of satellite altimetry (Fu and Cazenave, 2001). From an orbit of approximately 1,300 km, satellite altimeters can measure sea surface heights averaged over an area of several square kilometers with an accuracy of about 1 cm. This accuracy implies that any oceanographic phenomenon with a sea surface height (SSH) signature, including tides, can be examined in satellite altimeter data. Global barotropic tide models that are developed from satellite altimeter data (e.g., Egbert et al., 1994; Ray, 1999) compare extremely well to independent observations such as tide gauges and bottom pressure recorders (Shum et al., 1997). Because tides contribute about 80% of the SSH variance measured by altimeters, examination of nontidal oceanic motions in altimeter data can only take place after tides have been accurately removed from altimeter records (Le Provost, 2001). This illustrates a fundamental truth about the place of tides in physical oceanography: they are "signal" in many applications, and "noise" in many other applications. Satellite altimeters have also been instrumental in the study of internal tides. Although internal tides take on their greatest amplitudes at depth, their signature in altimeter data is large enough to be detectable (e.g., Ray and Mitchum, 1996, 1997).

Barotropic tides generate internal tides, and internal tides in turn feed back onto the barotropic tides. Inferences from altimetry-constrained barotropic tide models show that about one-third of global tidal energy dissipation occurs in regions of rough topography, where internal tides are generated (Egbert and Ray, 2000). Internal tide generation thus acts as a damping mechanism for the barotropic tides.

Figure 1a,b shows the surface elevation amplitude of the principal lunar semidiurnal tide M_2, the largest tidal constituent in the ocean. Figure 1a displays the M_2 amplitude in TPXO (Egbert et al., 1994), a highly accurate altimetry-constrained barotropic tide model. Figure 1b displays the M_2 amplitude in the new concurrent HYbrid Coordinate Ocean Model (HYCOM) simulations described in this paper. Although the HYCOM M_2 amplitudes are clearly very similar to those in TPXO, they are less accurate due to the lack of constraints applied using satellite altimetry. (Thus far, our HYCOM simulations are "forward" simulations, that is, simulations unconstrained by data.) Another key difference is that the HYCOM simulations include internal tides, which can be
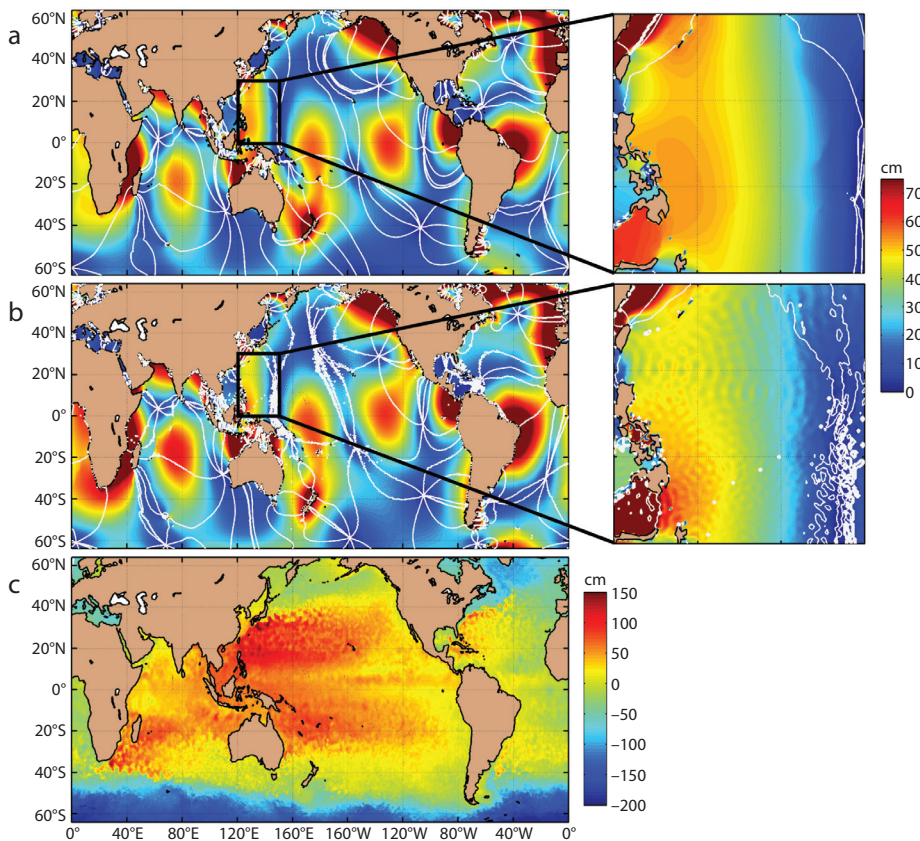

Figure 1. (a) Amplitude (cm) of M_2 surface tidal elevation in TPXO (Egbert et al., 1994), a highly accurate barotropic tide model constrained by satellite altimetry. (b) Amplitude (cm) of M_2 surface tidal elevation in HYbrid Coordinate Ocean Model (HYCOM) simulations in which the tide is unconstrained by satellite altimetry. White lines in (a) and (b) indicate lines of constant phase. Insets to the right of (a) and (b) display amplitude and phase in the western Pacific region delineated by boxes in (a) and (b). (c) January 19, 2012, snapshot of sea surface height (cm) in the real-time data-assimilative HYCOM without tides.

seen in Figure 1b as small-scale "wiggles" in the lines of constant phase (white lines in Figure 1a,b) and as small-scale "dimples" in the amplitude contours of Figure 1b. The presence of internal tide perturbations to amplitude and phase in the new concurrent HYCOM simulation, and the lack of these perturbations in TPXO, is more easily seen by contrasting the insets to Figure 1a,b. The insets focus on the western Pacific, a region of strong internal tides.

GLOBAL GENERAL CIRCULATION MODELING

With the notable exception of gravitationally forced ocean tides, the atmosphere provides the primary forcing of large-scale motions in the ocean (motions on scales from 1 km up to basin scales). For instance, exchanges between the ocean and atmosphere at the sea surface exert a strong control on ocean stratification. Seawater is stratified by density, and seawater density is a function of temperature, salinity, and pressure. Temperatures in the upper ocean (and lower atmosphere) are determined by fluxes of sensible and latent heat between the atmosphere and ocean (Yu and Weller, 2007). Salinities in the upper ocean are set by the difference between evaporation and precipitation at the ocean surface (Yu, 2007; Schmitt, 2008). Because the buoyancy (density) of seawater at the ocean surface is controlled by temperature and salinity, the forcing described above is known as buoyancy forcing. The atmosphere forces the ocean through pressure loading (Ponte, 1993) and wind stress (Pond and Pickard, 1983) in addition to the buoyancy forcing. Wind stress at the ocean surface drives near-inertial motions (Alford, 2003; Simmons and

Alford, 2012, in this issue), Ekman flows (Pedlosky, 1996), and the large-scale general circulation (Pedlosky, 1996). Winds blowing on the sea surface also drive oceanic motions on small scales (scales from about 1 cm to about 1 km), such as capillary waves (Cox, 1958), surface wind waves (Phillips, 1966), and Langmuir cells (Langmuir, 1938). These small-scale motions, however, are not resolved in models such as HYCOM, which make the hydrostatic approximation (Pedlosky, 1987; Vallis, 2006).

The oceanic general circulation consists of the well-known current systems around the globe, such as the Gulf Stream in the western North Atlantic Ocean, the Kuroshio in the western North Pacific Ocean, the Agulhas Current off of Southern Africa, and the Antarctic Circumpolar Current in the Southern Ocean (Schmitz, 1996a,b; Siedler et al., 2001). On timescales of about 10–200 days, these currents meander and generate highly energetic mesoscale eddies (Schmitz, 1996a,b; Stammer, 1997), the spinning oceanic dynamical counterparts of atmospheric weather systems generated through a hydrodynamical process known as baroclinic instability (Pedlosky, 1987; Vallis, 2006). Because currents meander and mesoscale eddies are born and die over relatively long timescales (scales much longer than, for instance, tidal timescales), these currents and eddies are sometimes referred to as low-frequency motions.

A substantial percentage of the kinetic energy in the ocean resides in mesoscale eddies and other transient low-frequency features such as current meanders. Because the horizontal length scales of strong currents and mesoscale eddies are relatively small (about 100 km), numerical models of the ocean must have high

resolution in order for the modeled low-frequency kinetic energies to compare well to those recorded in observations from satellite altimeters and other instruments (Hurlburt and Hogan, 2000; Maltrud and McClean, 2005). The grid spacing in current state-of-the-art global high-resolution ocean models is about 1/10° to 1/12°, which is thought to be sufficient to capture most of the oceanic mesoscale. Indeed, ocean models having resolutions this high or higher are known as "eddying" models (Hecht and Hasumi, 2008). Note, however, that Thoppil et al. (2011) find that increasing the resolution of HYCOM from 1/12° to 1/25° yields further increases in the energy of modeled low-frequency flows, suggesting that resolutions of 1/25° or higher might be necessary to fully resolve mesoscale eddies and current meanders.

HYCOM is currently being developed for use as the next-generation global ocean forecast model for the United States Navy (Chassignet et al., 2007; Metzger et al., 2010; http://hycom. org; http://www7320.nrlssc.navy.mil/ GLBhycom1-12). The Navy needs to know the state of the ocean—the strength of currents, sea surface height, clarity of the water, and sound propagation properties, among others—on a range of temporal and spatial scales at diverse locations around the globe. The model is forced by fluxes obtained from the Navy Operational Global Atmospheric Prediction System (NOGAPS; Rosmond et al., 2002). The data-assimilative version of the model uses satellite altimetric sea surface height, radiometric sea surface temperature, and in situ ship, float, and profile temperature and salinity data using the Navy Coupled Ocean Data Assimilation system (NCODA; Cummings, 2005) to provide a statistical

blending of model and observations. The global ocean model runs on a combination Mercator and combination tripolar grid (Murray, 1996) and Mercator grid with an equatorial grid resolution of 0.08° (8.9 km) and is coupled to a sea ice model at high latitudes. HYCOM simulations at 0.04° (4.5 km) have already begun to be developed and run. The model reproduces the general circulation of the global ocean, the strength and variability of western boundary currents such as the Gulf Stream and the Kuroshio, and the mesoscale eddies generated by instabilities of the major currents. The model is validated by comparison to in situ observations not used in assimilation (Hurlburt et al., 2010; Thoppil et al., 2011). The global model performance is not as good in coastal regions where smaller-scale features in bathymetry, and new phenomena such as tides, become important in determining the state of the ocean.

To contrast nontidal and tidal SSH fields, Figure 1c displays a snapshot of SSH in the data assimilative (ocean forecasting) version of HYCOM, which currently does not include tides. The relatively high sea surface heights in the subtropical regions are the subtropical gyres (Pedlosky, 1996). The strongest gradients in sea surface height take place in western boundary currents such as the Gulf Stream and the Kuroshio. The numerous small-scale features present in Figure 1c are the oceanic mesoscale eddies.

MARRIAGE OF GLOBAL TIDAL AND GENERAL CIRCULATION MODELING

Recently, we have shown that tides and the atmospherically forced eddying ocean general circulation can be modeled concurrently on a global scale; hence, tides and nontidal motions now interact in the model, as in the ocean. We add astronomical tidal forcing of the four largest semidiurnal constituents (M_2, S_2, N_2, and K_2) and the four largest diurnal constituents (K_1, O_1, P_1, and Q_1) to the HYCOM general circulation model, which is also forced by atmospheric fields as discussed in the previous section. Arbic et al. (2010) offer more details of the new concurrent tidally and atmospherically forced simulations. Here, we note that we use the parameterized topographic internal wave drag scheme of Garner (2005), modified as described in Arbic et al. (2010), in order to limit the maximum decay rates to (9 hrs)$^{-1}$. The wave drag scheme parameterizes the drag on tidal flows resulting from the generation of unresolved small-vertical-scale internal waves by tidal flow over rough topography. Because the wave drag acting on tidal motions is known to have a different strength than the wave drag acting on nontidal motions (Bell, 1975), we separate the tidal and nontidal bottom flows in our model using a 25-hour running boxcar filter. The self-attraction and loading term (Hendershott, 1972) is simplified using the scalar approximation (Ray, 1998) and is applied only to the nonsteric component of sea surface height, which is dominated by the large-scale barotropic tides.

With these adaptations, HYCOM generates both barotropic and internal tides amidst the eddying general circulation. The barotropic tides in the new concurrent HYCOM tidal simulations were compared against the standard set of 102 pelagic tide gauges (Shum et al., 1997) in Arbic et al. (2010), who found that HYCOM captured about 93% of the sea surface elevation variance of the eight largest tidal constituents in the tide gauge records. Arbic et al. (2010; see their Figure 3) showed that the nontidal sea surface height variability was not adversely affected by the presence of tides in the model. In the new concurrent HYCOM tidal simulations, in contrast to early internal tide simulations (Arbic et al., 2004; Simmons et al., 2004), the atmospheric forcing present permits a realistic horizontally varying stratification in the ocean model. As a result, the internal tides in high latitudes are generated in a stratification that is more realistic than was possible in early internal tide simulations. In Figure 2, we display the consequences of this horizontally varying stratification for M_2. The figure displays the amplitude of the M_2 internal tide signature in the steric sea surface height (i.e., the sea surface height component having to do with stratification effects). Figure 2a, taken from a HYCOM simulation like those in earlier global internal tide studies—using a two-layer, horizontally uniform stratification typical of the subtropics—displays an artificially strong internal tide in high-latitude regions such as the Labrador Sea and Drake Passage. In the new concurrent HYCOM simulations with tides embedded within an atmospherically forced model (Figure 2b), this defect is removed. Figure 2b also demonstrates that the introduction of a more realistic 32-layer horizontally varying stratification leads to increased internal tide amplitudes at most of the major generation sites in the mid- and low-latitude oceans, when compared to the internal tides generated in a two-layer horizontally uniform stratification. See, for instance, the area around Hawai'i.

Using the new concurrent tide model,

we have begun to examine a host of scientific and operational questions about internal tides. In the following sections, we give brief overviews of some of our preliminary results of this exploration.

GLOBAL COMPARISON OF MODELED INTERNAL TIDES WITH SATELLITE ALTIMETER ESTIMATES

We have begun to validate the internal tides in our model with a global comparison to satellite altimeter observations. As in the previous section, we focus here on M_2, the largest constituent of oceanic tides. We apply a 50–400 km band-pass filter to the M_2 amplitudes at the sea surface in order to remove both small-horizontal-scale noise (in the altimeter data) and large-scale barotropic tides (in the altimeter data and in the HYCOM simulation). The band passing therefore leaves only the low-mode internal tide remaining. Figure 3 displays the results of applying the band-pass filter to the surface M_2 elevations. Figure 3a displays results from along-track satellite altimeter data (Ray and Mitchum, 1996, 1997; Richard Ray, NASA, *pers. comm.*, 2011), while Figure 3b displays results from the model output interpolated to the same altimeter tracks. The "hotspots" of internal tide generation at prominent topographic features such as Hawai'i and the Aleutians in the North Pacific, the Tuamotu Archipelago in the South Pacific, Madagascar in the Indian Ocean, and so on, are very clearly seen in both panels of Figure 3. The internal waves radiate away from the hotspots as focused beams, which propagate for thousands of kilometers. The magnitudes of the internal tide perturbations to M_2 sea surface elevations are typically about 1 cm or more in the hotspot regions. We

averaged the root-mean-square (rms) perturbation magnitudes over the five hotspot regions delineated by boxes in Figure 3b, and found that the modeled rms values agree with the altimeter rms

values to within about 20% over these regions. All of this supports further confidence in the realism of the internal tides in our HYCOM simulations, in the same manner that side-by-side
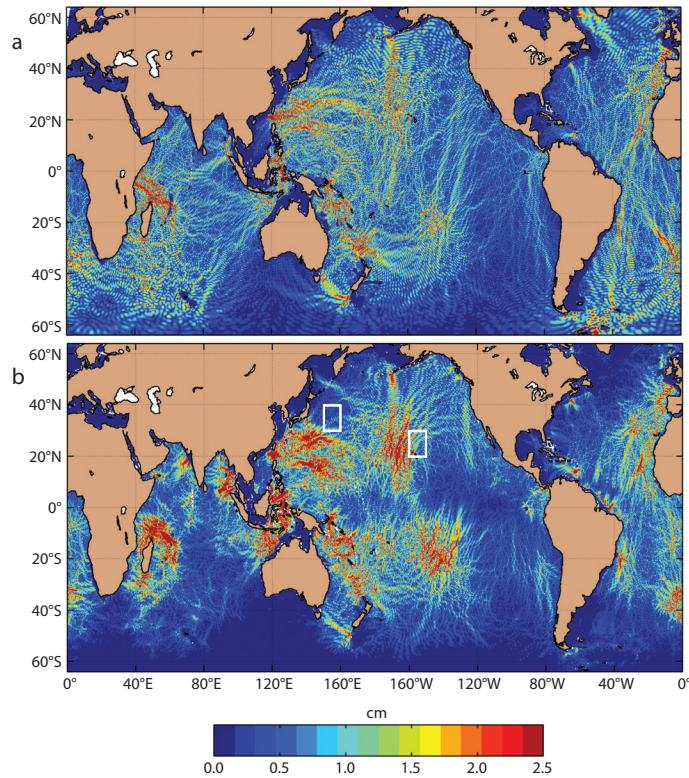

Figure 2. Amplitude (cm) of the M_2 internal tide signature in steric sea surface height of HYCOM experiments (a) run as in early internal tide simulations with M_2 tidal forcing as the only forcing present and with a horizontally uniform two-layer stratification, (b) run with astronomical tidal forcing present amongst an atmospherically forced 32-layer general circulation model with horizontally nonuniform stratification. Boxes in Figure 2b denote regions over which wavenumber spectra are computed in Figure 4.
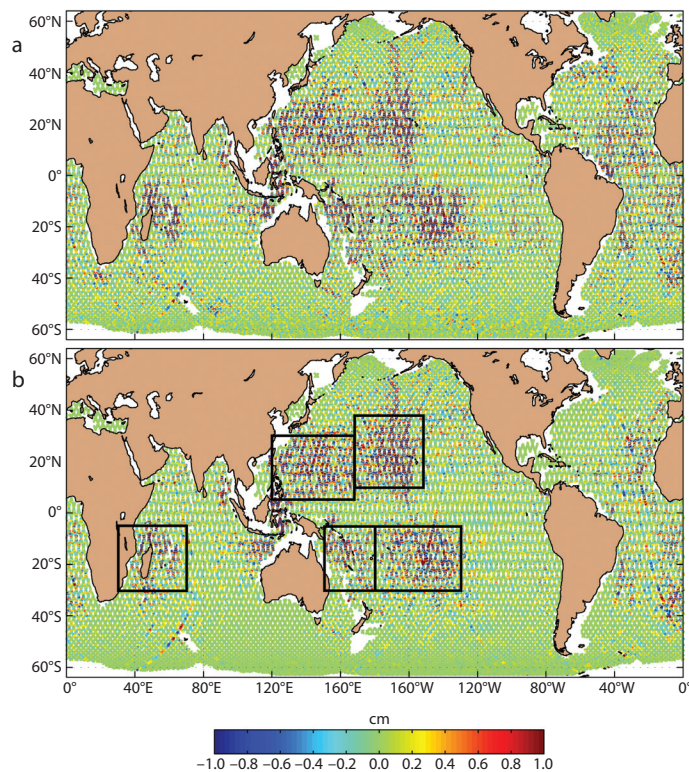

Figure 3. M_2 internal tide perturbation (cm) to sea surface elevation. Perturbations are determined via band passing the total M_2 sea surface elevation amplitude. (a) Results from analysis of along-track satellite altimeter data (Ray and Mitchum 1996, 1997; Richard Ray, NASA, *pers. comm.,* 2011). (b) Results from high-resolution simulation of HYCOM. The boxes in (b) delineate "hotspot" regions over which root-mean-square values of the internal tide perturbations are computed from both altimeter data and HYCOM output (see text).

plots of the low-frequency sea surface height variance in high-resolution models versus satellite altimeter data (see, for instance, Figure 12 in Maltrud and McClean, 2005) lend confidence in the ability of high-resolution models to simulate mesoscale eddies.

TIDAL AND NONTIDAL CONTRIBUTIONS TO THE SEA SURFACE HEIGHT SPECTRUM

We have begun to use our model to distinguish between the high-frequency tidal and low-frequency nontidal contributions to quantities of interest such as the wavenumber spectrum of sea surface height. Because the satellite altimeter repeats tracks every 10 days, high-frequency motions such as the tides are aliased into longer periods (Parke et al., 1987). In satellite altimeter data, therefore, it is sometimes difficult to distinguish between tidal motions and lower-frequency motions. Because our model output is written at hourly intervals, we can easily separate low- from high-frequency signals in the model. In Figure 4 we show the wavenumber spectrum of SSH from the model. The wavenumber spectrum measures the energy content of a signal as a function of wavenumber, which is inversely proportional to the wavelength. The slope of the wavenumber spectrum is of great theoretical interest, as it is used to infer the dominant dynamics of low-frequency flows (e.g., Le Traon et al., 2008; Xu and Fu, 2011). In regions where low-frequency motions are more energetic than tidal motions, such as the Kuroshio (see westernmost box in Figure 2b), low-frequency motions dominate the spectrum of total SSH (Figure 4a). However, in regions where internal tides are energetic, for instance near Hawai'i (see easternmost box in Figure 2b), high-frequency tidal motions dominate the high end of the wavenumber spectrum (Figure 4b). The latter observation implies that in data taken by the planned high-resolution wide-swath satellite altimeter (Fu and Ferrari, 2008), internal tides will have to be removed very accurately before low-frequency oceanic motions can be studied. Tides have always been an important source of noise in altimeter measurements of SSH. However, internal tides will become a more important source of noise for the wide-swath altimeter mission than for previous altimeter missions. This issue is due to the much higher spatial resolution of the wide-swath mission, which will collect data at horizontal scales where the internal tides contain substantial energy.

GLOBAL COMPARISON OF MODELED TIDAL CURRENTS WITH CURRENT METER OBSERVATIONS

We have begun to compare the tidal currents in our model to those in current meter observations. The set of current meter observations we use is built upon the current meter database in Scott et al. (2010), which includes observations from 1,528 locations, denoted by blue dots in Figure 5a. A total of 4,934 instruments are spread out over many depths at the 1,528 locations.

Because the ocean is stratified, tidal currents have vertical structure, just as tidal displacements do. In Figure 5b, we compare the vertical structure of the M_2 tidal kinetic energy in our HYCOM
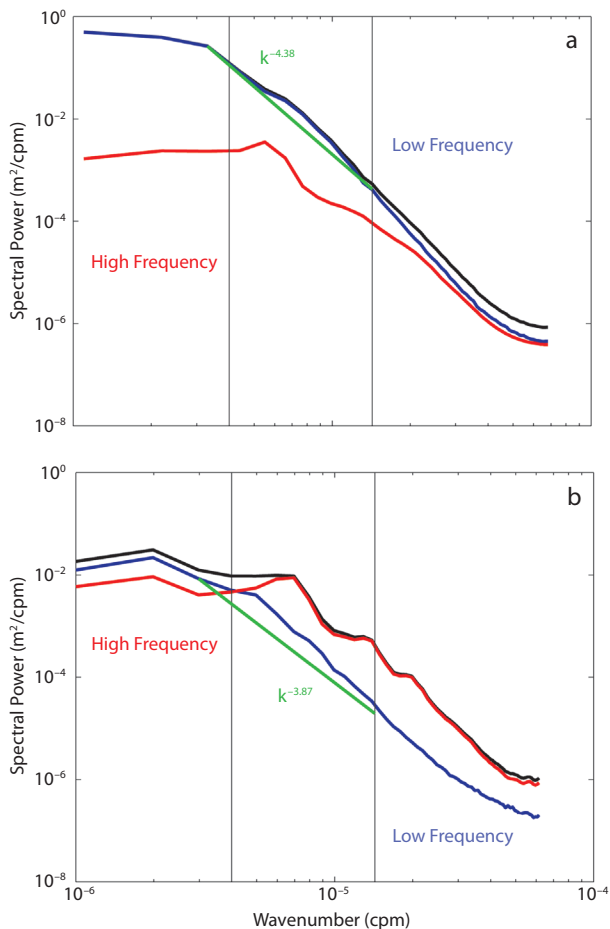

Figure 4. Wavenumber spectrum of total (black), high-frequency (red) and low-frequency (blue) sea surface height, where two days is the dividing point between low and high frequencies, for (a) Kuroshio region, a region of very strong low-frequency motions, and (b) region north of Hawai'i, in which low-frequency motions are weaker than M_2 internal tidal motions. The two regions are delineated by the westernmost and easternmost boxes, respectively, in the North Pacific in Figure 2b. Spectra are computed from a HYCOM simulation containing both tides and low-frequency atmospherically forced motions. Extra green lines are drawn in at the best-fit slopes of −4.38 and −3.87 over low-frequency motions in the same wavenumber band discussed in Xu and Fu (2011). As discussed in Le Traon et al. (2008) and Xu and Fu (2011), −11/3 and −5 slopes imply surface quasi-geostrophic and quasi-geostrophic dynamics, respectively.

simulations against that seen in the current meters. The time-averaged kinetic energy is calculated over the M_2 tidal period at each instrument location for both model output and current meter data, and then averaged over all locations having instruments within a specified depth range. As can be seen in Figure 5b, after this spatial averaging is performed, the model captures the vertical structure of the semidiurnal M_2 tide very well—having less than a 25% relative error in the top 2,000 m. We have completed a much more comprehensive model-data comparison for tidal currents in the North Atlantic (recent work of author Timko and colleagues) in which the observations have been divided on a regional basis. The study of the North Atlantic shows that model performance can vary significantly from one region to another. The cause of regional differences in model performance is a subject of future investigation.

Model diurnal kinetic energies appear substantially weaker than in observations (not shown). The cause appears to be that tuning the topographic internal wave drag for M_2 as we have done in Arbic et al. (2010) and here implies that the diurnal tides in the model are overdamped. Theoretical considerations (Bell, 1975) imply that the wave drag on diurnal motions is less strong than for semidiurnal motions. We are currently working to implement a frequency-dependent wave drag into the HYCOM simulations. It is not simple to do this, however, because the model runs in the time domain whereas semidiurnal and diurnal tides are most easily separated in the frequency domain.

IMPLICATIONS AND FUTURE DEVELOPMENTS

The development of a model with barotropic and internal tides embedded within an eddying ocean general circulation has opened up a host of scientific questions and applications, some of which are described in earlier sections of this paper. As discussed, the model is expected to be useful in planning for the next-generation wide-swath satellite altimeter (Fu and Ferrari, 2008). Indeed, the model already has been used to estimate the relative importance of tidal versus nontidal contributions to the wavenumber spectrum of sea surface height in the regions where a planned airborne test campaign will be undertaken (Ernesto Rodriguez, NASA, 2011, *pers. comm.*). Three-dimensional maps of tidal displacements and currents are potentially useful for removing tidal "noise" from data taken by various oceanographic instruments. In addition, the new concurrent tide model is being used in the Climate Process Team project "Collaborative Research: Representing Internal-Wave Driven Mixing in Global Ocean Models," which focuses on improving estimates of internal-wave-mediated mixing in the ocean. The project involves several institutions, Jennifer MacKinnon of the Scripps Institution of Oceanography leads the project, and the National Science Foundation funds it.
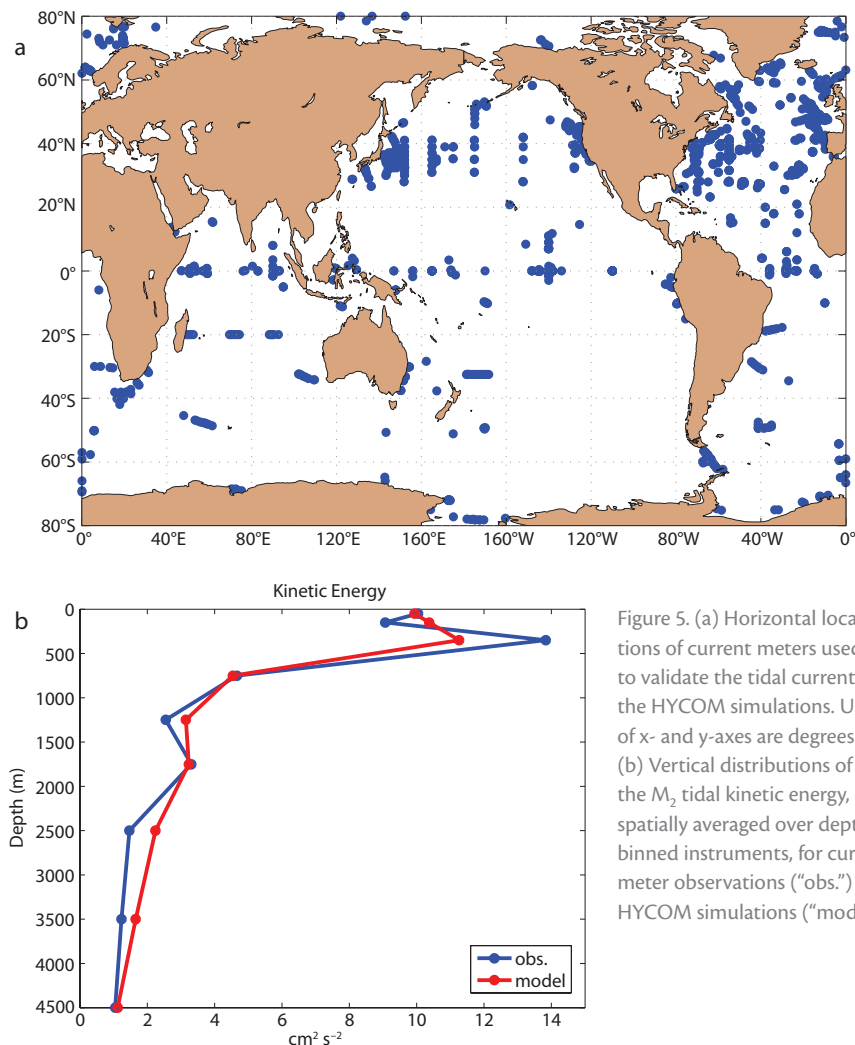
The new concurrent tide model is also

Figure 5. (a) Horizontal locations of current meters used to validate the tidal currents in the HYCOM simulations. Units of x- and y-axes are degrees. (b) Vertical distributions of the M_2 tidal kinetic energy, spatially averaged over depth-binned instruments, for current meter observations ("obs.") and HYCOM simulations ("model").

expected to be useful for regional and coastal modeling. Regional and coastal models often include tidal forcing, but this forcing is generally barotropic, such that internal tides are not included in the open boundary conditions. Kelly and Nash (2010) showed that the response of shelf tides to barotropic plus internal (i.e., fully three-dimensional) tidal forcing can be quite different from the response to forcing that includes only barotropic tides. The Australian North West Shelf is a region where a low vertical-mode internal tide is expected to propagate onto the shelf from the open ocean (Sam Kelly, University of Western Australia, *pers. comm.*, 2012). Current meter observations (Holloway et al., 2001) show propagation of a mode-1 internal tide onto the shelf. The global model at 4 km resolution underestimates the strength of the internal tide compared to the observations, but shows onshore propagation from deep water onto the shelf consistent with the observations. However, a regional model forced by barotropic tidal boundary conditions shows onshore propagation of the internal tide only inshore of the critical slope, and offshore propagation over the outer continental slope, in disagreement with the observations. By including tidal forcing in a fully three-dimensional global ocean circulation model, we will provide an internal tide capability everywhere, and allow nested models to include internal tides at their open boundaries.

A number of improvements are needed for the new concurrent tide model. The self-attraction and loading term (Hendershott, 1972) is implemented in a rather crude way, using the so-called scalar approximation (Ray, 1998), and it needs to be improved upon in future versions of the model. The

frequency dependence of topographic wave drag (Bell, 1975) is problematic because the model is run in the time domain, not the frequency domain. Perhaps the greatest technical challenge remaining is how to perform data assimilation on the tidal as well as nontidal motions within the model. Successful data assimilation, once performed, will make the model much more useful for operational purposes of the United States Navy and other users.

ACKNOWLEDGEMENTS

REFERENCES
Alford, M.H. 2003. Improved global maps and 54-year history of wind-work on ocean inertial motions. *Geophysical Research Letters* 30, 1424, http://dx.doi.org/10.1029/2002GL016614.
Arbic, B.K., S.T. Garner, R.W. Hallberg, and H.L. Simmons. 2004. The accuracy of surface elevations in forward global barotropic and baroclinic tide models. *Deep-Sea Research Part II* 51:3,069–3,101, http://dx.doi.org/10.1016/j.dsr2.2004.09.014.

Arbic, B.K., A.J. Wallcraft, and E.J. Metzger. 2010. Concurrent simulation of the eddying general circulation and tides in a global ocean model. *Ocean Modelling* 32:175–187, http://dx.doi.org/10.1016/j.ocemod.2010.01.007.
Bell, T.H. 1975. Lee waves in stratified flows with simple harmonic time dependence. *Journal of Fluid Dynamics* 67:705–722, http://dx.doi.org/10.1017/S0022112075000560.
Carter, G.S., O.B. Fringer, and E.D. Zaron. 2012. Regional models of internal tides. *Oceanography* 25(2):56–65, http://dx.doi.org/10.5670/oceanog.2012.42.
Cartwright, D.E. 1999. *Tides: A Scientific History*. Cambridge University Press, Cambridge, 192 pp.
Chassignet, E.P., H.E. Hurlburt, O.M. Smedstad, G.R. Halliwell, P.J. Hogan, A.J. Wallcraft, R. Baraille, and R. Bleck. 2007. The HYCOM (HYbrid Coordinate Ocean Model) data assimilative system. *Journal of Marine Systems* 65:60–83, http://dx.doi.org/10.1016/j.jmarsys.2005.09.016.
Cox, C.S. 1958. Measurements of slopes of high frequency wind waves. *Journal of Marine Research* 16:199–225.
Cummings, J.A. 2005. Operational multivariate ocean data assimilation. *Quarterly Journal of the Royal Meteorological Society* 131: 3,583–3,604.
Egbert, G.D., A.F. Bennett, and M.G.G. Foreman. 1994. TOPEX/POSEIDON tides estimated using a global inverse model. *Journal of Geophysical Research* 99:24,821–24,852, http://dx.doi.org/10.1029/94JC01894.
Egbert, G.D., and R.D. Ray. 2000. Significant dissipation of tidal energy in the deep ocean inferred from satellite altimeter data. *Nature* 405:775–778, http://dx.doi.org/10.1038/35015531.
Fu, L.-L., and A. Cazenave, eds. 2001. *Satellite Altimetry and Earth Sciences: A Handbook of Techniques and Applications*. Academic Press, San Diego, 463 pp.
Fu, L.-L., and R. Ferrari. 2008. Observing oceanic submesoscale processes from space. *Eos, Transactions American Geophysical Union* 89(48), 488, http://dx.doi.org/10.1029/2008EO480003.
Garner, S.T. 2005. A topographic drag closure built on an analytical base flux. *Journal of the Atmospheric Sciences* 62:2,302–2,315, http://dx.doi.org/10.1175/JAS3496.1.
Hecht, M.W., and H. Hasumi, eds. 2008. *Ocean Modeling in an Eddying Regime.* Geophysical Monograph 177, American Geophysical Union, Washington, DC, 409 pp, http://dx.doi.org/10.1029/GM177.
Hendershott, M.C. 1972. The effects of solid earth deformation on global ocean tides. *Geophysical Journal of the Royal Astronomical Society* 29:389–402, http://dx.doi.org/10.1111/j.1365-246X.1972.tb06167.x.
Hibiya, T., M. Nagasawa, and Y. Niwa. 2006. Global mapping of diapycnal diffusivity in the deep ocean based on the results of expendable

current profiler (XCP) surveys. *Geophysical Research Letters* 33, L03611, http://dx.doi.org/10.1029/2005GL025218.

Holloway, P.E., P.G. Chatwin, and P. Craig. 2001. Internal tide observations from the Australian North West Shelf in summer 1995. *Journal of Physical Oceanography* 31:1,182–1,199, http://dx.doi.org/10.1175/1520-0485(2001)031<1182:ITOFTA>2.0.CO;2.

Hurlburt, H.E., and P.J. Hogan. 2000. Impact of 1/8° to 1/64° resolution on Gulf Stream model-data comparisons in basin-scale subtropical Atlantic Ocean models. *Dynamics of Atmospheres and Oceans* 32:283–329, http://dx.doi.org/10.1016/S0377-0265(00)00050-6.

Hurlburt, H.E., E.J. Metzger, J.G. Richman, E.P. Chassignet, Y. Drillet, M.W. Hecht, O. Le Galloudec, J.F. Shriver, X. Xu, and L. Zamudio. 2010. Dynamical evaluation of ocean models using the Gulf Stream as an example. Pp. 545–609 in *Operational Oceanography in the 21st Century*. G.B. Brassington and A. Schiller, eds, Springer-Verlag, New York.

Kelly, S.M., and J.D. Nash. 2010. Internal-tide generation and destruction by shoaling internal tides. *Geophysical Research Letters* 37, L23611, http://dx.doi.org/10.1029/2010GL045598.

Langmuir, I. 1938. Surface motion of water induced by wind. *Science* 87:119–123, http://dx.doi.org/10.1126/science.87.2250.119.

Le Provost, C. 2001. Ocean tides. Pp. 267–303 in *Satellite Altimetry and Earth Sciences: A Handbook of Techniques and Applications*. Academic Press, San Diego.

Le Traon, P.-Y., P. Klein, and B.-L. Hua. 2008. Do altimeter wavenumber spectra agree with the interior or surface quasi-geostrophic theory? *Journal of Physical Oceanography* 38:1,137–1,142, http://dx.doi.org/10.1175/2007JPO3806.1.

Maltrud, M.E., and J.L. McClean. 2005. An eddy resolving global 1/10° simulation. *Ocean Modelling* 8:31–54, http://dx.doi.org/10.1016/j.ocemod.2003.12.001.

Metzger, E.J., O.M. Smedstad, P.G. Thoppil, H.E. Hurlburt, D.S. Franklin, G. Peggion, J.F. Shriver, and A.J. Wallcraft. 2010. *Validation Test Report for the Global Ocean Forecast System V3.0 – 1/12° HYCOM/NCODA: Phase II*. Naval Research Laboratory, NRL/MR/7320—10-9236, 70 pp. Available online at: http://www7320.nrlssc.navy.mil/pubs/2010/metzger1-2010.pdf (accessed May 10, 2012).

Munk, W., and C. Wunsch. 1998. Abyssal recipes II: Energetics of tidal and wind mixing. *Deep-Sea Research Part I* 45:1,977–2,010, http://dx.doi.org/10.1016/S0967-0637(98)00070-3.

Murray, R.J. 1996. Explicit generation of orthogonal grids for ocean models. *Journal of Computational Physics* 126(2):251–273, http://dx.doi.org/10.1006/jcph.1996.0136.

Niwa, Y., and T. Hibiya. 2011. Estimation of baroclinic tide energy available for deep ocean mixing based on three-dimensional global numerical simulations. *Journal of Oceanography* 67:493–502, http://dx.doi.org/10.1007/s10872-011-0052-1.

Padman, L., S. Howard, and R. Muench. 2006. Internal tide generation along the South Scotia Ridge. *Deep-Sea Research Part II* 53:157–171, http://dx.doi.org/10.1016/j.dsr2.2005.07.011.

Parke, M.E., R.H. Stewart, D.L. Farless, and D.E. Cartwright. 1987. On the choice of orbits for an altimetric satellite to study ocean circulation and tides. *Journal of Geophysical Research* 92:11,693–11,707, http://dx.doi.org/10.1029/JC092iC11p11693.

Pedlosky, J. 1987. *Geophysical Fluid Dynamics*. Springer-Verlag, Berlin, 710 pp.

Pedlosky, J. 1996. *Ocean Circulation Theory*. Springer-Verlag, Berlin, 453 pp.

Phillips, O.M. 1966. *The Dynamics of the Upper Ocean*. Cambridge University Press, New York, 269 pp.

Pond, S., and G.L. Pickard. 1983. *Introductory Dynamical Oceanography*, Second Edition. Pergamon Press, Oxford, 329 pp.

Ponte, R.M. 1993. Variability in a homogeneous global ocean forced by barometric pressure. *Dynamics of Atmospheres and Oceans* 18(3–4):209–234, http://dx.doi.org/10.1016/0377-0265(93)90010-5.

Ray, R.D. 1998. Ocean self-attraction and loading in numerical tidal models. *Marine Geodesy* 21:181–191, http://dx.doi.org/10.1080/01490419809388134.

Ray, R.D. 1999. *A Global Ocean Tide Model From TOPEX/POSEIDON Altimetry: GOT99.2*. National Aeronautics and Space Administration Technical Memorandum, NASA/TM-1999-209478, 58 pp.

Ray, R.D., and G.T. Mitchum. 1996. Surface manifestation of internal tides generated near Hawai'i. *Geophysical Research Letters* 23:2,101–2,104, http://dx.doi.org/10.1029/96GL02050.

Ray, R.D., and G.T. Mitchum. 1997. Surface manifestation of internal tides in the deep ocean: Observations from altimetry and tide gauges. *Progress in Oceanography* 40:135–162, http://dx.doi.org/10.1016/S0079-6611(97)00025-6.

Rosmond, T.E., J. Teixeira, M. Peng, T.F. Hogan, and R. Pauley. 2002. Navy Operational Global Atmospheric Prediction System (NOGAPS): Forcing for ocean models. *Oceanography* 15(1):99–108, http://dx.doi.org/10.5670/oceanog.2002.40.

Schmitt, R.W. 2008. Salinity and the global water cycle. *Oceanography* 21(1):12–19, http://dx.doi.org/10.5670/oceanog.2008.63.

Schmitz, W.J. Jr. 1996a. *On the World Ocean Circulation: Volume I, Some Global Features/North Atlantic Circulation*. Woods Hole Oceanographic Institution Technical Report WHOI-96-03, 140 pp.

Schmitz, W.J. Jr. 1996b. *On the World Ocean Circulation: Volume II, The Pacific and Indian Oceans/A Global Update*. Woods Hole Oceanographic Institution Technical Report WHOI-96-08, 237 pp.

Scott, R.B., B.K. Arbic, E.P. Chassignet, A.C. Coward, M. Maltrud, W.J. Merryfield, A. Srinivasan, and A. Varghese. 2010. Total kinetic energy in four global eddying ocean circulation models and over 5000 current meter records. *Ocean Modelling* 32:157–169, http://dx.doi.org/10.1016/j.ocemod.2010.01.005.

Shum, C.K., P.L. Woodworth, O.B. Andersen, G.D. Egbert, O. Francis, C. King, S.M. Klosko, C. Le Provost, X. Li, J.-M. Molines, and others. 1997. Accuracy assessment of recent ocean tide models. *Journal of Geophysical Research* 102:25,173–25,194, http://dx.doi.org/10.1029/97JC00445.

Siedler, G., J. Church, and J. Gould. 2001. *Ocean Circulation and Climate: Observing and Modeling the Global Ocean*. Academic Press, San Diego, 715 pp.

Simmons, H.L., R.W. Hallberg, and B.K. Arbic. 2004. Internal wave generation in a global baroclinic tide model. *Deep-Sea Research Part II* 51:3,043–3,068, http://dx.doi.org/10.1016/j.dsr2.2004.09.015.

Simmons, H.L. 2008. Spectral modification and geographic redistribution of the semi-diurnal internal tide. *Ocean Modelling* 21:126–138, http://dx.doi.org/10.1016/j.ocemod.2008.01.002.

Simmons, H.L., and M.H. Alford. 2012. Simulating the long-range swell of internal waves generated by ocean storms. *Oceanography* 25(2):30–41, http://dx.doi.org/10.5670/oceanog.2012.39.

Stammer, D. 1997. Global characteristics of ocean variability estimated from regional TOPEX/Poseidon altimeter measurements. *Journal of Physical Oceanography* 27:1,743–1,769, http://dx.doi.org/10.1175/1520-0485(1997)027<1743:GCOOVE>2.0.CO;2.

Thoppil, P.G., J.G. Richman, and P.J. Hogan. 2011. Energetics of a global ocean circulation model compared to observations. *Geophysical Research Letters* 38, L15607, http://dx.doi.org/10.1029/2011GL048347.

Vallis, G.K. 2006. *Atmospheric and Oceanic Fluid Dynamics: Fundamentals and Large-Scale Circulation*. Cambridge University Press, Cambridge, 745 pp.

Wunsch, C. 1975. Internal tides in the ocean. *Reviews of Geophysics* 13:167–182, http://dx.doi.org/10.1029/RG013i001p00167.

Xu, Y., and L.-L. Fu. 2011. Global variability of the wavenumber spectrum of oceanic mesoscale turbulence. *Journal of Physical Oceanography* 41:802–809, http://dx.doi.org/10.1175/2010JPO4558.1.

Yu, L. 2007. Global variations in oceanic evaporation (1958–2005): The role of changing wind speed. *Journal of Climate* 20:5,376–5,390, http://dx.doi.org/10.1175/2007JCLI1714.1.

Yu, L., and R.A. Weller. 2007. Objectively analyzed air-sea heat fluxes for the global ice-free oceans (1981–2005). *Bulletin of the American Meteorological Society* 88:527–539, http://dx.doi.org/10.1175/BAMS-88-4-527.